Design of Chirped Gratings Using Interferometric Lithography
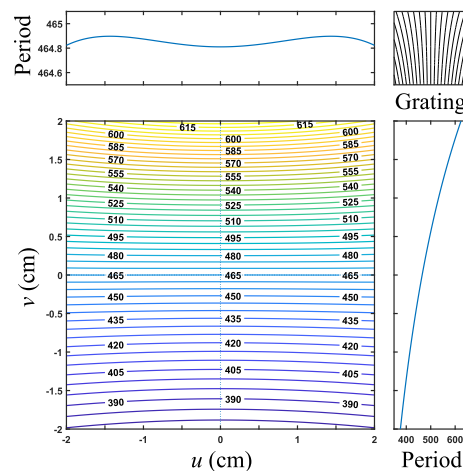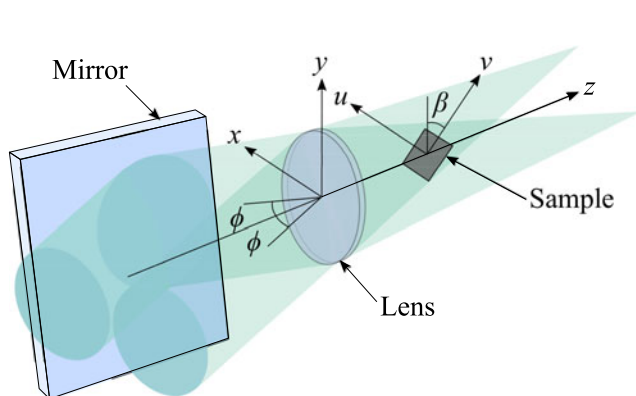
Steve Benoit
S. R. J. Brueck, *Life Fellow, IEEE*

Design of Chirped Gratings Using Interferometric Lithography

Steve Benoit [1] **and S. R. J. Brueck** ,[2] *Life Fellow, IEEE*

[1]Department of Mathematics, Colorado State University, Fort Collins, CO 80521 USA
[2]Department of Electrical and Computer Engineering and the Center for High Technology
Materials, University of New Mexico, Albuquerque, NM 87106 USA

Abstract: Interferometric lithography with curved wavefronts produces chirped gratings. The chirp can be longitudinal, with the periodicity changing along the grating wavevector, or transverse, with the periodicity changing in the perpendicular direction. The chirp is investigated for a range of configurations, and specific optical systems to generate a wide range of grating chirp parameters are analyzed.

Index Terms: Chirped grating, interferometric lithography.

1. Introduction

Periodic structures have many uses in photonics [1], [2]. One-dimensional structures (gratings) are used to provide optical dispersion, for coupling to waveguides in integrated optics, for DFB/DBR lasers, for optical coatings and many other applications. Two-dimensional structures are important for photonic crystals and photonic and meta-surfaces. Three-dimensional periodic structures form the basis of photonic crystals and volume Bragg reflectors. Both the linear and the nonlinear properties of these structures have been investigated over a wide range of materials.

Nearly periodic, chirped gratings have also been investigated for pulse compression [3], for fiber communications and sensing [4], [5], for controlling distributed feedback lasers [6], and for nonlinear optics [7]. There are applications for both transverse chirped gratings where the dominant chirp is in the direction perpendicular to the grating wavevector and for longitudinal chirped gratings where the dominant chirp is in the same direction as the grating wavevector. For many applications, the ratio of these two chirps is an important figure of merit for the grating fabrication method.

There have been many investigations of using interferometric lithography (IL) to produce periodic gratings [8], [9]. Fewer studies are available on the use of IL for chirped gratings [10]–[13]. The concept is straightforward, introduce an optical element into one or both interferometric beams to change the wavefront from the flat wavefront of a plane wave to a complex wavefront that changes across the photosensitive surface. A spherical lens is used to provide a 2D variation while a cylindrical lens provides a 1D wavefront variation. The position and orientation of the photosensitive surface also impacts the final chirp parameters.

Recent papers have demonstrated a dynamic tuning capability for a mid-IR semiconductor laser using a grating chirped in the transverse direction, perpendicular to the grating wavevector [14]. To accommodate the full width of the semiconductor, the longitudinal chirp, perpendicular to the
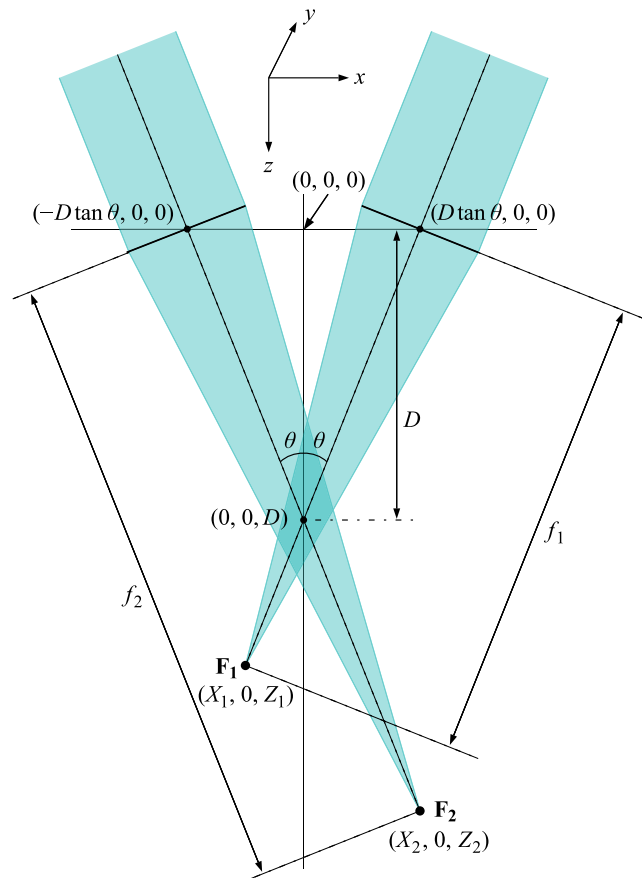
Fig. 1. General arrangement for creating chirped gratings by interferometric lithography. Coordinates are chosen so optical axes lie in the xz-plane, intersect each other at $(0, 0, D)$, with focal points/lines at $\mathbf{F}_i = (X_i, 0, Z_i)$, where $X_i = \pm D \tan\theta \mp f_i \sin\theta$ and $Z_i = f_i \cos\theta$. The two beams are assumed coherent throughout the interference volume indicated by the darker shade. The lenses can be either spherical or cylindrical and cylindrical lenses can be oriented with focal lines at any angle relative to the y-axis.

grating lines had to be limited to less than the DFB bandwidth[15]. Two figures of merit (FoM) were introduced to characterize the chirp, the ratio of transverse to longitudinal chirp from the center to each edge of the chip area, and the ratio of the distributed feedback stop band width to the longitudinal chirp. In this paper, we consider only the first FoM since the second includes specifics of the laser modal calculation, while this paper is focused on the broader issue of the application specific control of the chirp.

The paper is organized as follows. Section 2 describes the volumetric interference patterns for the geometries we consider: spherical lenses and cylindrical lenses with focal lines oriented at some angle to the plane formed by their optical axes. Section 3 describes an experimental configuration using a single lens to produce interfering wavefronts. Sections 4–7 describe the specifics of the grating patterns written in these geometries. Finally, Section 8 discusses conclusions and the further application of these techniques to general chirped grating design.

2. General Interferometric Configuration

Chirped gratings result from the interference of two coherent beams with curved wavefronts. A general configuration is shown in Fig. 1. Two collimated beams are incident onto individual lenses whose optical axes define a plane. Interference is possible throughout the volumetric extension of

the dark shaded region of Fig. 1 and the sample can be placed anywhere inside this region. The lenses may be spherical or cylindrical and there is no necessary relationship between their focal lengths.

In the following, we reference distances from an idealized focal point, but recognize that focusing to a point is limited by both lens aberrations and diffraction. The wavefronts produced by a lens are very nearly spherical or cylindrical at large distances (relative to the confocal parameter of the beam) from the focal point. Aberrations may distort a pattern, but will not alter the central period or impact the overall period variation except at the edges of the pattern. In our analysis, we use the focal point of rays entering nearly normal to the lens surface, which is accurate for rays near the center of the exposure region.

For spherical lenses, the distance from the respective focal points to any point (x, y, z) in space is given by

$$l_i^{sph} = \sqrt{(X_i - x)^2 + y^2 + (Z_i - z)^2} \quad i \in \{1, 2\}, \tag{1}$$

and the corresponding $\vec{k}$-vectors for the converging wavefronts are given by

$$\vec{k}_i^{sph} = \frac{2\pi}{\lambda} \frac{1}{l_i^{sph}} \left[\hat{e}_x(X_i - x) + \hat{e}_y(-y) + \hat{e}_z(Z_i - z) \right]. \tag{2}$$

If cylindrical lenses are used, the lenses may be oriented so that their focal lines lie in the xz-plane, or may be rotated as much as 90° about their axis so that the focal lines are parallel to the y-axis. Let α denote the rotation angle of a cylindrical lens, where $\alpha = 0$ corresponds to focal lines in the xz-plane and $\alpha = 90°$ corresponds to focal lines parallel to the y-axis. We assume lenses remain reflection-symmetric across the yz-plane, with focal lines parallel to $\hat{v}_i = (\pm \cos\theta \cos\alpha, \sin\alpha, \sin\theta \cos\alpha)$. For such a lens configuration,

$$l_i^{cyl\text{-}\alpha} = \sqrt{(X_i - x)^2 + y^2 + (Z_i - z)^2 - \varsigma_i^2},$$

$$\vec{k}_i^{cyl\text{-}\alpha} = \frac{2\pi}{\lambda} \frac{1}{l_i^{cyl\text{-}\alpha}} \left[\hat{e}_x(X_i - x - \varsigma_i \cos\theta \cos\alpha) + \hat{e}_y(-y \mp \varsigma_i \sin\alpha) + \hat{e}_z(Z_i - z \mp \varsigma_i \sin\theta \cos\alpha) \right], \tag{3}$$

where $\varsigma_i = (X_i - x)\cos\theta\cos\alpha \mp y \sin\alpha \pm (Z_i - z)\sin\theta\cos\alpha$.

In particular, when focal lines are parallel to the y-axis, with $\alpha = 90°$, then $\varsigma_i = \mp y$ and the results are

$$l_i^{cyl\text{-}y} = \sqrt{(X_i - x)^2 + (Z_i - z)^2},$$

$$\vec{k}_i^{cyl\text{-}y} = \frac{2\pi}{\lambda} \frac{1}{l_i^{cyl\text{-}y}} \left[\hat{e}_x(X_i - x) + \hat{e}_z(Z_i - z) \right], \tag{4}$$

and when focal lines lie in the xz-plane with $\alpha = 0$, the results are

$$l_i^{cyl\text{-}xz} = \sqrt{\xi_i^2 + y^2},$$

$$\vec{k}_i^{cyl\text{-}xz} = \frac{2\pi}{\lambda} \frac{1}{l_i^{cyl\text{-}xz}} \left[\hat{e}_x(\xi_i \sin\theta) - \hat{e}_y(y) \mp \hat{e}_z(\xi_i \cos\theta) \right], \tag{5}$$

where $\xi_i \equiv (X_i - x)\sin\theta \mp (Z_i - z)\cos\theta$.

In the following sections, these expressions are examined to illustrate the accessible chirp parameter space.

3. Single Lens Configuration

Consider the specific variation of Fig. 1 consisting of a Lloyd mirror and single plano-convex lens mounted on a rotating stage, shown in Fig. 2(a). The system is illuminated by a coherent source,
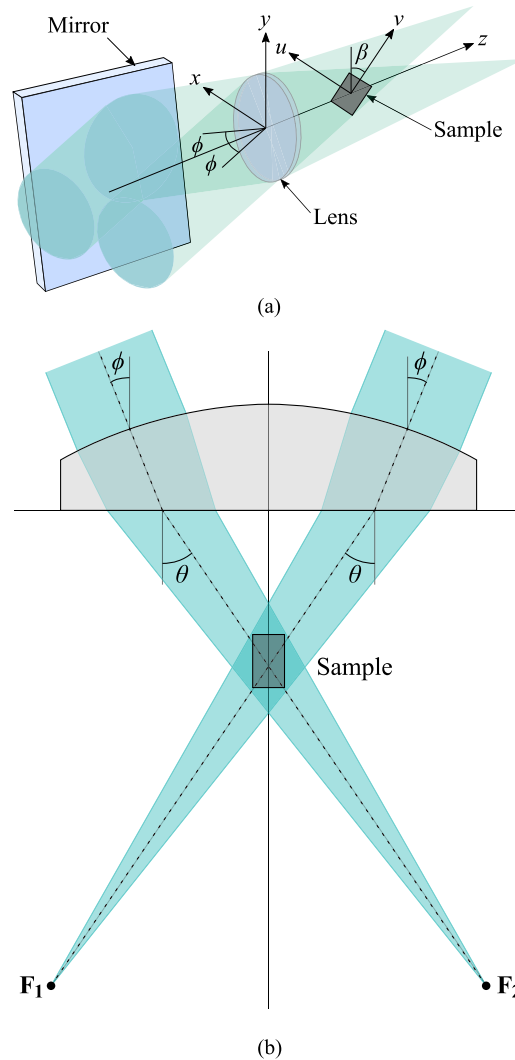
Fig. 2. (a) Interferometric lithography (IL) configuration with Lloyd mirror, lens, and sample placement; (b) Schematic view with foci positions, normal incident angle ϕ, refracted angle θ, and sample placement indicated.

producing an interference pattern of two converging wavefronts in the region behind the lens, which can be transferred onto a planar sample coated with photoresist that is oriented at an angle β from the y-axis. The significance of β will be discussed below. In Fig. 2, the incident illumination is shown as two separated beams; experimentally, a single larger incident beam is used. IL requires transverse coherence (e.g. a nearly single-mode beam) and longitudinal coherence to within any path length differences associated with the optical system over the interference area. Without the lens, independent of the tilt of the sample, this is a traditional Lloyd's mirror configuration [8] and the grating period is given by

$$P = \frac{\lambda}{2 \sin \phi}.$$ (6)

For a lens with center thickness t, radius R, and material refractive index n, and for plane waves incident at angle ϕ, rays entering the lens normal to its surface have exit angle θ and coordinates
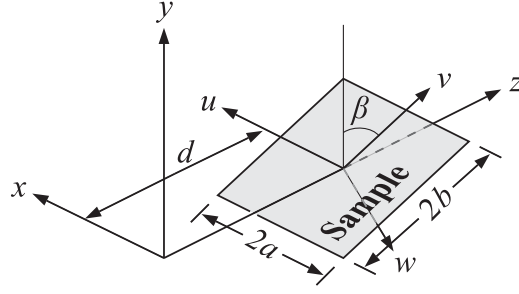
Fig. 3. Sample coordinate system. (u, v) sample coordinates have origin on the z-axis at $z = D$, u lies in the xz-plane, and v lies in the yz-plane, at an angle β from the y-axis. Sample dimensions are $2a \times 2b$, as shown.

of the resulting foci given by

$$Z_i = \left(\frac{R \cos \phi}{(n-1)n} + \frac{R-t}{n} \right) \eta^{3/2},$$

$$X_i = \pm \frac{(R-t)(n^2-1)\tan^3 \phi}{\cos \phi} \mp \frac{R \sin \phi}{n-1} \eta,$$

$$\theta = \sin^{-1}(n \sin \phi),$$

$$D = (R-t)\frac{\tan \phi}{\tan \theta}, \qquad (7)$$

where $\eta = (1 - n^2 \sin^2 \phi)/\cos^2 \phi$.

When deriving grating patterns, we assume the light arriving at each focus has the same phase; in practice, phases will differ but this should only result in phase offsets in derived interference patterns (e.g. shifts of the interference pattern modulo the grating period).

3.1 Sample Placement

The next step is to specialize to a planar sample surface tilted at an angle β from the xy-plane. We define a second coordinate system, as shown in Fig. 3, tied to the sample surface, whose coordinates are given as $(u, v, w = 0)$, and whose origin lies a distance D from the origin of the (x, y, z) coordinate system (the center of the back face of the lens, under the configuration in Fig. 2) and where the u-axis is parallel to the x-axis of the lens coordinate system. A point (u, v) in the sample plane has (x, y, z) spatial coordinates $(u, v\cos \beta, D + v\sin \beta)$. The unit vectors in these systems are related by the simple rotational transform

$$\{\hat{e}_x = \hat{e}_u; \hat{e}_y = \cos \beta \hat{e}_v - \sin \beta \hat{e}_w; \hat{e}_z = \sin \beta \hat{e}_v + \cos \beta \hat{e}_w\}.$$

3.2 Grating Period and Chirp

For any of the lens configurations we consider, if we define $L(u, v) = l_1(u, v) - l_2(u, v)$ as the path length difference from the two foci to a point (u, v) on the sample, then the local grating period at that point is given by

$$P(u, v) = \frac{\lambda}{|\nabla L(u, v)|},$$

where the gradient

$$\nabla L(u, v) = \left(\partial_u L(u, v), \partial_v L(u, v) \right)$$

gives the grating wavevector direction normal to the grating lines. The period in the u and v directions are given by

$$P_u(u, v) = \frac{\lambda}{|\partial_u L(u, v)|}, \quad \text{and } P_v(u, v) = \frac{\lambda}{|\partial_v L(u, v)|}, \tag{8}$$

which imply that

$$\frac{1}{P(u, v)} = \sqrt{\frac{1}{P_u^2(u, v)} + \frac{1}{P_v^2(u, v)}}. \tag{9}$$

Chirp is a measure of change in period across the grating. For a grating with dimension $2a$ in the u direction and $2b$ in the v direction, as shown in Fig. 3, we define chirps in the u and v directions as

$$C_u = P(a, 0) - P(0, 0), \quad \text{and } C_v = P(0, b) - P(0, 0).$$

We will refer to a figure of merit (FoM) defined as the magnitude of the ratio of these chirps:

$$\text{FoM} = \left| \frac{C_v}{C_u} \right| = \left| \frac{P(0, b) - P(0, 0)}{P(a, 0) - P(0, 0)} \right|. \tag{10}$$

Maximizing this value will maximize transverse chirp while minimizing longitudinal chirp and vice versa.

4. Spherical Lens Configuration

When a positive spherical lens is used, the spherical waves converge toward the foci. The distances l_i from each of the two foci to a point (u, v) on the sample are given by

$$l_i^{sph}(u, v) = \sqrt{(X_i - u)^2 + (v \cos \beta)^2 + (Z_i - D - v \sin \beta)^2},$$

and the corresponding wavevectors are

$$\vec{k}_i^{sph}(u, v) = \frac{2\pi}{\lambda} \frac{1}{l_i^{sph}(u, v)} \left[\hat{e}_x(X_i - u) + \hat{e}_y(-v \cos \beta) + \hat{e}_z(Z_i - D - v \sin \beta) \right]$$

$$= \frac{2\pi}{\lambda} \frac{1}{l_i^{sph}(u, v)} \left[\hat{e}_u(X_i - u) + \hat{e}_v((Z_i - D) \sin \beta - v) + \hat{e}_w((Z_i - D) \cos \beta) \right].$$

Then the grating period in the u direction is

$$P_u^{sph}(u, v) = \frac{\lambda}{\left| \frac{X_1 - u}{l_1^{sph}(u, v)} - \frac{X_2 - u}{l_2^{sph}(u, v)} \right|}, \tag{11}$$

and in the v direction,

$$P_v^{sph}(u, v) = \frac{\lambda}{\left| \frac{v - (Z_1 - D) \sin \beta}{l_1^{sph}(u, v)} - \frac{v - (Z_2 - D) \sin \beta}{l_2^{sph}(u, v)} \right|}. \tag{12}$$

The local grating period is given by (9). In the special case shown in Fig. 2, where $X \equiv X_2 = -X_1$ and $Z \equiv Z_1 = Z_2$, the period at the grating center, $u = v = 0$, is

$$P^{sph}(0, 0) = \frac{\lambda \sqrt{X^2 + (Z - D)^2}}{2X}. \tag{13}$$

Note that for $\beta = 0$, the sample normal to the optical axis, (11) and (12) are even in u and v, and an approximately quadratic period dependence is expected in both directions. However, for $\beta \neq 0$, P_u has a linear variation with v, while it remains quadratic in u. P_v remains even in both u and v.
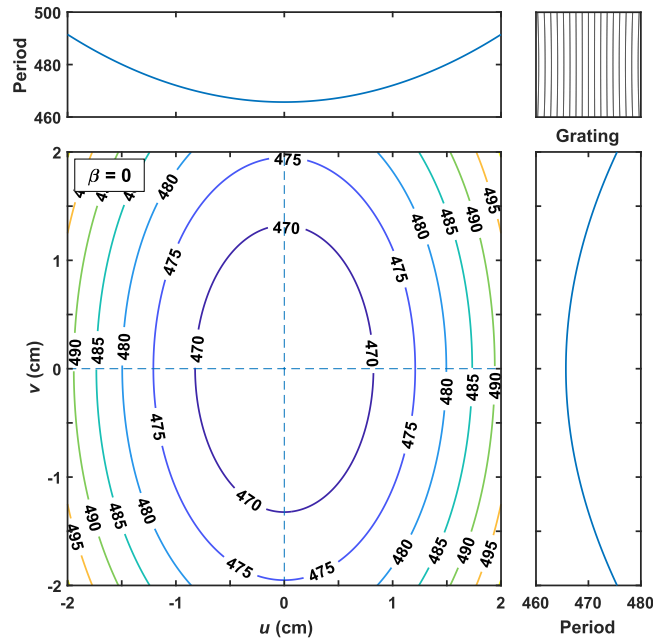
Fig. 4. Contours of constant period for sample normal to the optical axis. Other parameters as given in the text. The smaller plots show the variation in u and v along the dotted lines passing through the optical axis ($u = v = 0$). The inset shows grating line orientation, with one grating line per 5000 drawn.

Fig. 4 shows the period variation across a 4 cm $\times$ 4 cm sample for $\lambda = 355$ nm, using a lens with $f = 163$ mm ($R = 77.35$ mm, $t = 7$ mm), $\phi = 15°$, ($\theta = 22.4°$) and $\beta = 0$ (sample normal to optical axis), for which $Z_i \approx 135.4$ mm, $X_i \approx \mp 37$ mm, and $D \approx 45.7$ mm. Without the lens, this configuration would give a uniform grating with a period of 686 nm. Since the grating structure is close to a simple grating oriented in the v direction, the variation is dominated by the P_u term given by (11). As is easily seen from Fig. 2, the lens results in an increase in the incident angle at the center of the sample, and hence a reduced pitch of 465.5 nm, given by $P(0, 0) = \lambda / [2 \sin(\tan^{-1} \frac{X_1}{Z_1 - D})]$. The period variation is even and approximately quadratic in both u and v with a larger chirp in the u direction, FoM $= 0.38$.

For $\beta = 45°$, a much larger variation of the period across the v axis is obtained as shown in Fig. 5. The range of grating periods along the v-direction is greatly increased as a result of the tilt while the variation along u is largely unchanged. In terms of the FoM defined above, FoM$|_{\beta=0} = 0.38$ while FoM$|_{\beta=45°} = 3.17$. The FoM can be increased by shifting the sample in the v-direction relative to the optical axis, as long as the sample remains in the region of interference. Even larger FoMs are available by further increasing β. The practical limitations are the variation of the intensity on the photoresist vs. v and the high reflectivity from the photoresist surface at large β. The range of grating periods along $u = 0$ can be evaluated from (11),

$$P_u^{sph}(0, v) = \frac{\lambda}{\left| \frac{X_1}{l_1^{sph}(0, v)} - \frac{X_2}{l_2^{sph}(0, v)} \right|}, \tag{14}$$

providing a simple expression for evaluating the available transverse chirp as the optical parameters are varied.

Experimentally, we verified these results for $\beta = 45°$, a lens with $f = 37.5$ mm, $d = 2$ mm, and $\theta = 21°$; very good agreement was obtained between the calculated and measured grating periods across the wafer [15].
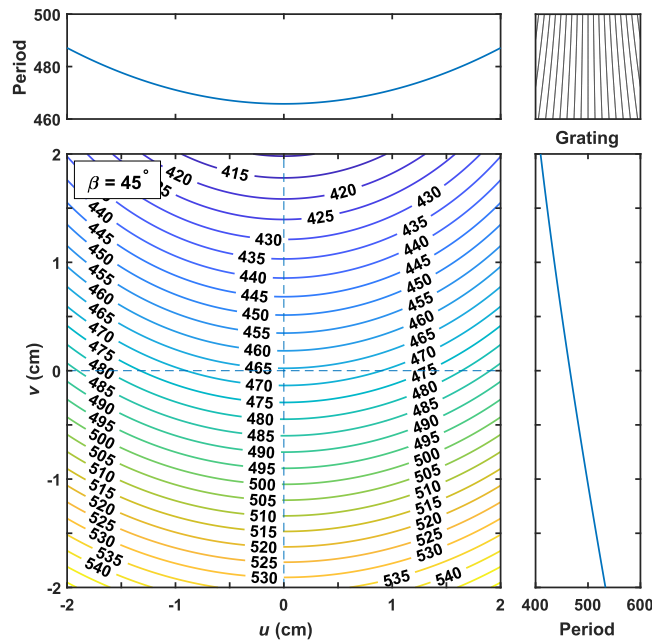
Fig. 5. Contours of constant period for $\beta = 45°$ with the same parameters as Fig. 4. The period variation in v is greatly increased and is close to linear with height.

This period variation is a result of the focusing of the lens across the face of the sample. The period at the center of the sample is unchanged from the normal incidence case, closer to the lens, negative v, the period is reduced while it is increased for positive v (larger angles of incidence).

5. Cylindrical Lens Configuration (Focal Lines in y-Direction)

Next we consider a configuration as in Fig. 1 with cylindrical lenses oriented such that the focal lines are parallel to the y-axis. Specializing (4) to the $(u, v, 0)$ plane gives

$$l_i^{cyl\text{-}y} = \sqrt{(X_i - u)^2 + (Z_i - D - v \sin \beta)^2},$$

$$\vec{k}_i^{cyl\text{-}y} = \frac{2\pi}{\lambda} \frac{1}{l_i^{cyl\text{-}y}} \left[\hat{e}_u(X_i - u) + \hat{e}_v(Z_i - D - v \sin \beta) \sin \beta + \hat{e}_w(Z_i - D - v \sin \beta) \cos \beta \right],$$

with the resulting period in the u and v directions given by

$$P_u^{cyl\text{-}y}(u, v) = \frac{\lambda}{\left| \dfrac{X_1 - u}{l_1^{cyl\text{-}y}(u,v)} - \dfrac{X_2 - u}{l_2^{cyl\text{-}y}(u,v)} \right|},$$

$$P_v^{cyl\text{-}y}(u, v) = \frac{\lambda}{\left| \dfrac{Z_1 - D - v \sin \beta}{l_1^{cyl\text{-}y}(u,v)} - \dfrac{Z_2 - D - v \sin \beta}{l_2^{cyl\text{-}y}(u,v)} \right| \sin \beta}. \tag{15}$$

The grating center period $P^{cyl\text{-}y}(0, 0)$ when $X \equiv X_2 = -X_1$ and $Z \equiv Z_1 = Z_2$ is identical to $P^{sph}(0, 0)$ in (13). Note that $P_v^{cyl\text{-}y} \to \infty$ as $\beta \to 0$. This implies a strictly longitudinal chirp with only a u-dependence in this special case.

With a single cylindrical lens arranged as in Fig. 2, gratings produced on tilted samples are very similar to those produced by spherical lenses. Using separate cylindrical lenses of differing focal length can generate gratings with chirp only in the v-direction [10]. Fig. 6 shows the calculated
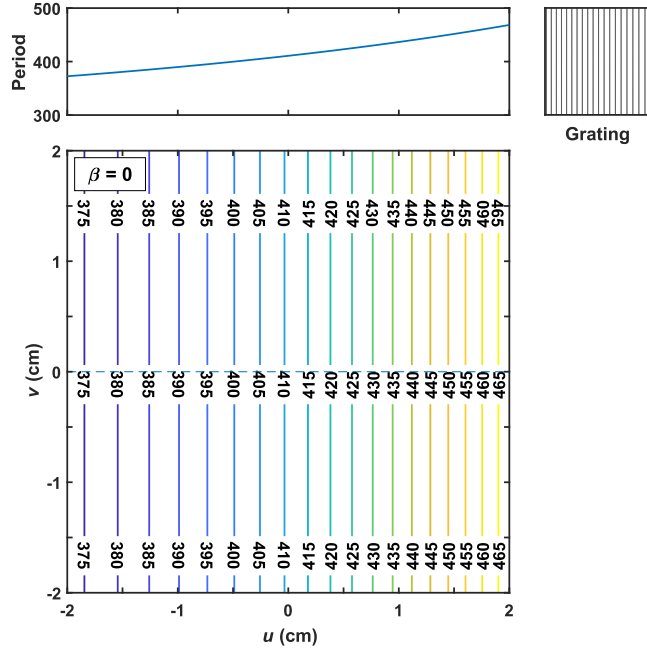
Fig. 6. Strictly longitudinal chirped grating formed by using cylindrical lenses with focal lengths of 20 and 200 cm at $\alpha = 0$, $\beta = 0$, $\theta = 25.6°$ and $D = 5$ cm. The top panel shows the period variation across the sample, which is nearly linear in u and independent of v.

period variation for the case of $f_1 = 20$ cm and $f_2 = 200$ cm, $\beta = 0$, $\theta = 25.6°$, $D = 5$ cm. The top panel is the variation along $v = 0$ showing a nearly linearly varying, purely longitudinal chirp.

6. Cylindrical Lens Configuration (Focal Lines in *xz*-Plane)

When two cylindrical lenses are oriented with focal lines in the *xz*-plane, there is very little variation in the period near the origin of the *uv*-plane and for $\beta = 0$, the variation is quadratic for $u, v \ll f$. Adding a tilt of the sample ($\beta \neq 0$) adds a linear variation along the *v*-axis as before.

Writing (5) in terms of sample coordinates provides explicit expressions for the period variation,

$$l_i^{cyl\text{-}xz} = \sqrt{\xi_i^2 + (v \cos \beta)^2},$$

$$\vec{k}_i^{cyl\text{-}xz} = \frac{2\pi}{\lambda} \frac{1}{l_i^{cyl\text{-}xz}} \left[\hat{e}_u(\xi_i \sin \theta) - \hat{e}_v(v \cos^2 \beta \pm \xi_i \cos \theta \sin \beta) + \hat{e}_w(v \sin \beta \mp \xi_i \cos \theta) \cos \beta \right],$$

where $\xi_i = (X_i - u) \sin \theta \mp (Z_i - D - v \sin \beta) \cos \theta$.

The resulting period in the u and v directions given by

$$P_u^{cyl\text{-}xz}(u, v) = \frac{\lambda}{\left| \frac{\xi_1}{l_1^{cyl\text{-}xz}(u,v)} - \frac{\xi_2}{l_2^{cyl\text{-}xz}(u,v)} \right| \sin \theta},$$

$$P_v^{cyl\text{-}xz}(u, v) = \frac{\lambda}{\left| \frac{\xi_1 \sin \beta \cos \theta + v \cos^2 \beta}{l_1^{cyl\text{-}xz}(u,v)} + \frac{\xi_2 \sin \beta \cos \theta + v \cos^2 \beta}{l_2^{cyl\text{-}xz}(u,v)} \right|}, \tag{16}$$

with grating center period $P^{cyl\text{-}xz}(0, 0)$ given by (6) with $\phi = \theta$ when $X \equiv X_2 = -X_1$ and $Z \equiv Z_1 = Z_2$.

This period variation is plotted in Fig. 7 for the specific case of $f = 16.2$ cm ($R_1 = R_2 = 7.7$ cm, $t = 7$ mm), $\theta = 15°$ and $\beta = 45°$. There is a large region near the optical axis that shows very little
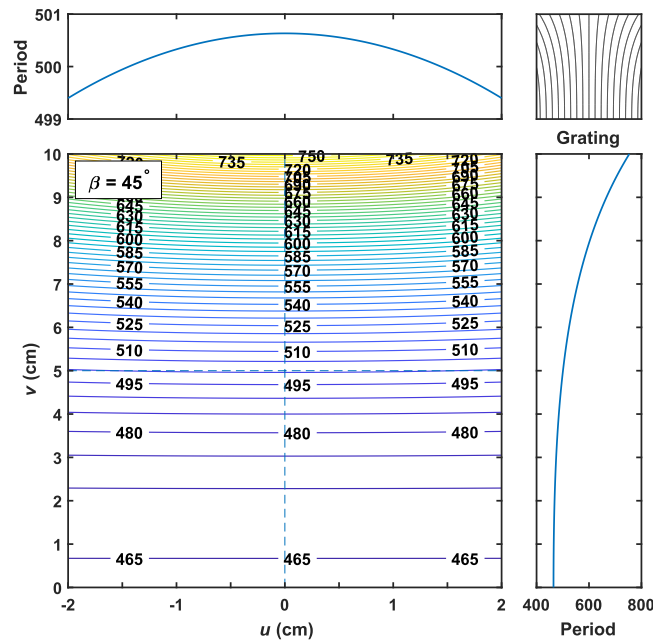
Fig. 7. Chirped grating formed for the *cyl-xz* geometry with the same lens parameters used in Fig. 5. Note that the chirp is quite small on the optical axis and increases dramatically for large offsets which are difficult to arrange experimentally.

chirp in either direction. For $\beta = 0$, as in the spherical lens case, the period variation is even in both u and v.

7. Cylindrical Lens Configuration (Focal Lines Rotated by Angle α)

The most general configuration we consider is a rotation of the focal lines of a pair of cylindrical lenses through an arbitrary angle α, as described in (3). With respect to (u, v) coordinates,

$$\ell_i^{cyl-\alpha} = \sqrt{(X_i - u)^2 + (v\cos\beta)^2 + (Z_i - D - v\sin\beta)^2 - \zeta_i^2}$$

$$\vec{k}_i^{cyl-\alpha} = \frac{2\pi}{\lambda}\frac{1}{\ell_i^{cyl-\alpha}}\left[\begin{array}{c} \hat{e}_x\big((X_i - u) - \zeta_i\cos\theta\cos\alpha\big) \\ + \hat{e}_y\big(-v\cos\beta \mp \zeta_i\sin\alpha\big) \\ + \hat{e}_z\big((Z_i - D - v\sin\beta) \mp \zeta_i\sin\theta\cos\alpha\big) \end{array}\right]$$

where $\zeta_i = (X_i - u)\cos\theta\cos\alpha \mp v\cos\beta\sin\alpha \pm (Z_i - D - v\sin\beta)\sin\theta\cos\alpha$. The resulting period in the u and v directions given by

$$P_u^{cyl-\alpha}(u, v) = \frac{\lambda}{\left|\dfrac{X_1 - u - \zeta_1\cos\theta\cos\alpha}{\ell_1^{cyl-\alpha}(u,v)} - \dfrac{X_2 - u - \zeta_2\cos\theta\cos\alpha}{\ell_2^{cyl-\alpha}(u,v)}\right|}$$

$$P_v^{cyl-\alpha}(u, v) = \frac{\lambda}{\left|\dfrac{v - (Z_1 - D)\sin\beta + Q_1}{\ell_1^{cyl-\alpha}(u,v)} - \dfrac{v - (Z_2 - D)\sin\beta - Q_2}{\ell_2^{cyl-\alpha}(u,v)}\right|} \tag{17}$$

where $Q_i = \zeta_i(\cos\beta\sin\alpha + \sin\beta\sin\theta\cos\alpha)$.

The period at the center of the grating, assuming $X_2 = -X_1$ and $Z_2 = Z_1$ is given by

$$P^{cyl-\alpha}(0, 0) = \frac{\lambda\sqrt{X^2 + (Z - D)^2 - \zeta_1^2}}{2(X - \zeta_1\cos\theta\cos\alpha)} \tag{18}$$
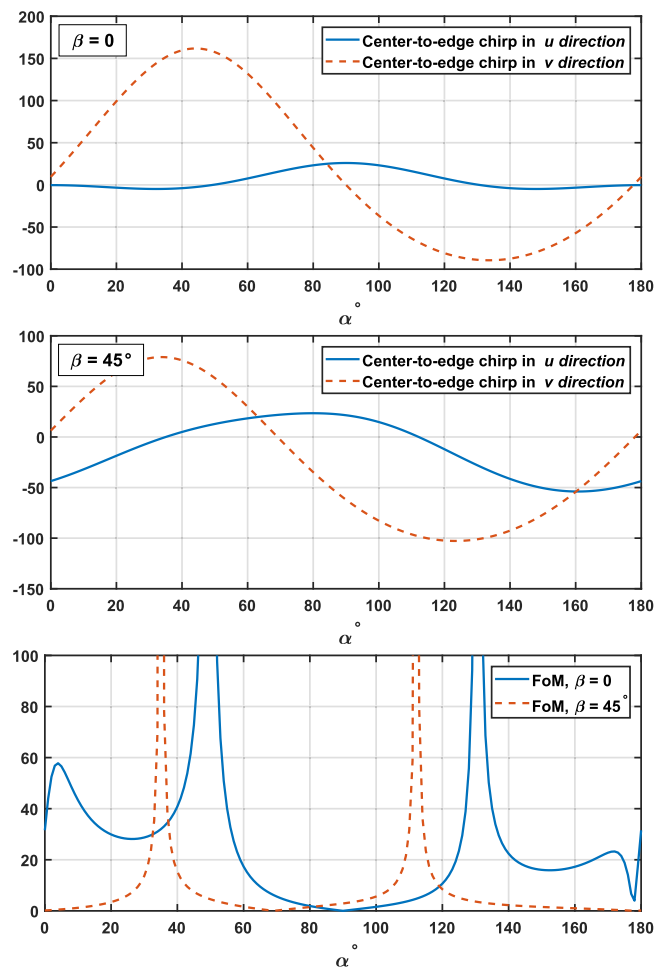
Fig. 8. Achievable transverse and longitudinal chirp using two cylindrical lenses with focal lines forming angle α with the xz-plane, where $\alpha = 90°$ corresponds to the *cyl-y* configuration of Section 5, and $\alpha = 0$ corresponds to the *cyl-xz* configuration of Section 6. Top panel shows configuration with $\beta = 0$, center panel shows configuration with $\beta = 45°$, and bottom panel shows dependence of FoM for both configurations for a 4×4 cm^2 sample.

The total achievable transverse chirp across a sample (along $u = 0$) depends strongly on α. Fig. 8 shows the relationship between the period change from the center to the edge of a 4 cm $\times$ 4 cm sample along the u and v directions using two cylindrical lenses with the same parameters as in Fig. 7, and for two configurations: $\beta = 0$ and $\beta = 45°$. Evidently a greater chirp can be obtained with $\beta = 0$, and in fact, maximal chirp was obtained in this configuration when $\beta = -12°$.

With this choice of lenses, maximal transverse chirp occurs for $\beta = 0$ when $\alpha \approx 49.18°$. Strong peaks in FoM occur at angles where longitudinal chirp is near zero, due to the definition of FoM as a ratio, but the chirps themselves vary smoothly, and are not overly sensitive to small variance in angle.

Fig. 9 shows the period variation for this system when $\alpha = 49.18°$, very near the peak of the graph in Fig. 8 (an angle for which lens focal lines intersect in the region of positive y). This configuration has nearly zero chirp in the u direction, resulting in a FoM on the order of 10^5; this should be compared with the FoM of 3.17 for the spherical lens case with shorter focal length lenses.
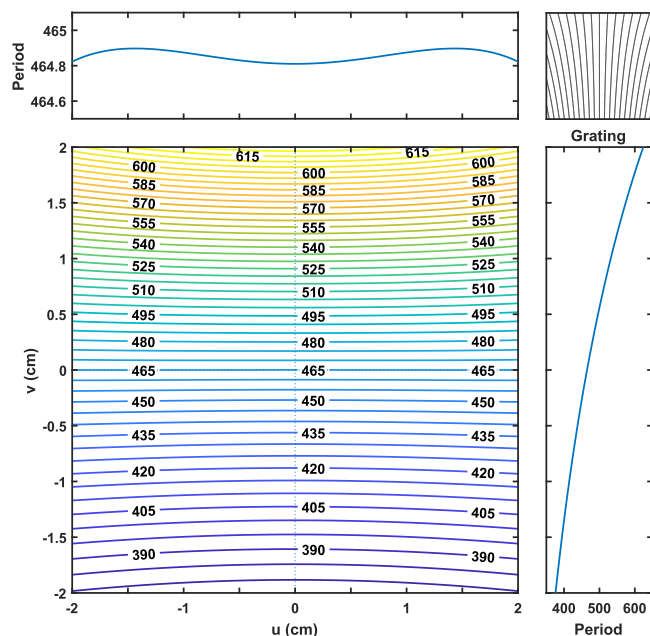
Fig. 9. Period variation for two cylindrical lenses oriented with $\alpha = 49.18°$ and $\beta = 0$.

8. Conclusions

In summary, we have shown that chirped gratings with a wide range of parameters from purely longitudinal to purely transverse can be fabricated using interferometric lithography. These capabilities will be important for a wide range of applications.

Specific applications will require that transverse and longitudinal chirp fall in desired ranges over a sample of particular size, and may require a degree of linearity in transverse chirp across a sample. To design a grating, incident light wavelength λ, lens geometry (R and t) and lens placement and orientation (θ and D) can be selected to achieve the desired center period, and the space of available chirps and period variations can be explored to find a grating with the desired properties. In general, reducing β will reduce variations in exposure intensity across the sample and increase overall exposure of photoresist by reducing reflection. The size of lens used and choice of D and θ allow control of the available size of the interference region, or the maximum size of the sample.

As the parameter space for design of an IL apparatus to create a desired grating is large, consisting of discrete options for λ, lens shape, R, and t and a continuum of available θ, D, α, and β, it is reasonable to develop software tools to automate the search over parameter space for suitable configurations.

References

[1] K. Busch, G. von Freymann, S. Linden, S. F. Mingaleev, L. Tkeshelashvili, and M. Wegener, "Periodic nanotructures for photonics," *Phys. Rep.*, vol. 444, no. 3, pp. 101–202, 2007.
[2] R. Halir *et al.*, "Waveguide sub-wavelength structures: a review of principles and applications," *Laser Photon. Rev.*, vol. 9, no. 1, pp. 25–49, 2015.
[3] G. Steinmeyer, "A review of ultrafast optics and optoelectronics," *J. Opt. A, Pure Appl. Opt.*, vol. 5, pp. R1–R15, 2003.
[4] H. Ishio, J. Minowa, and K. Nosu, "Review and status of wavelength-division-multiplexing technology and its application," *J. Lightw. Technol.*, vol. 2, no. 4, pp. 448–463, Aug. 1984.
[5] K. Hill and G. Meltz, "Fiber Bragg grating technology fundamentals and overview," *J. Lightw. Technol.*, vol. 15, no. 8, pp. 1263–1276, Aug. 1997.
[6] G. Agrawal and A. Bobeck, "Modeling of distributed feedback semiconductor lasers with axially-varying parameters," *IEEE J. Quantum Electron.*, vol. 24, no. 12, pp. 2407–2414, Dec. 1988.

[7] M. Charbonneau-Lefort, B. Afeyan, and M. Fejer, "Optical parametric amplifiers using chirped quasi-phase-matching gratings I: Practical design formulas," *J. Opt. Soc. Amer. B*, vol. 25, no. 4, pp. 463–480, 2008.
[8] S. Brueck, "Optical and interferometric lithography—Nanotechnology enablers," *Proc. IEEE*, vol. 93, no. 10, pp. 1704–1721, Oct. 2005.
[9] D. Xia, Z. Ku, S. Lee, and S. Brueck, "Nanostructures and functional materials fabricated by interferometric lithography," *Adv. Mater.*, vol. 23, pp. 147–179, 2011.
[10] A. Katzir, A. Livanos, and A. Yariv, "Chirped-grating output couplers in dielectric waveguides," *Appl. Phys. Lett.*, vol. 30, no. 5, pp. 225–226, 1977.
[11] Y. Liu, L. Zhang, and I. Bennion, "Fabricating fibre edge filters with arbitrary spectral response based on tilted chirped grating structures," *Meas. Sci. Technol.*, vol. 10, no. 1, pp. L1–L3, 1999.
[12] X. Mai, R. Moshrefzadeh, U. J. Gibson, G. I. Stegeman, and C. T. Seaton, "Simple versatile method for fabricating guided-wave gratings," *Appl. Opt.*, vol. 24, no. 19, pp. 3155–3161, 1985.
[13] H. Kim, H. Jung, D.-H. Lee, K. B. Lee, and H. Jeon, "Period-chirped gratings fabricated by laser interference lithography with a concave Lloyds mirror," *Appl. Opt.*, vol. 55, no. 2, pp. 354–359, 2016.
[14] L. Xue, S. Brueck, and R. Kaspi, "Widely tunable distributed-feedback lasers with chirped gratings," *Appl. Phys. Lett.*, vol. 94, 2009, Art. no. 161102.
[15] X. He, S. Benoit, R. Kaspi, and S. Brueck, "Optically pumped continuously tunable mid-IR distributed-feedback semiconductor laser," *IEEE J. Quantum Electron.*, vol. 52, no. 10, Oct. 2016, Art. no. 2200210.